Universitetet i Stavanger

FACULTY OF SCIENCE AND TECHNOLOGY

MASTER'S THESIS

Study program/specialization:	Spring semester, 2012
	~~Open~~ / Confidential
Author:	
Mihreteab Serekebirhan Teklehaimanot	…………………………………………
	(signature author)
Instructor : Arild Buland, PHD, Professor II	
Supervisor(e): Arild Buland, PHD, Professor II	
Title of Master's Thesis: Seismic reservoir characterization: Norwegian sea, Norway	
Norwegian title:	
ECTS: 30	

Subject headings:	
Reservoir characterization	Pages: …………………
Extended elastic Impedance	
Coloured inversion	+ Attachments/other: …………
Inversion	
Net pay	Stavanger. …………………
	date/year

ABSTRACT

A three step work flow seismic reservoir characterization method, comprised of the extended elastic impedance, coloured inversion and net pay estimation was tested in a data obtained from the western part of the deep water Vøring basin in the Norwegians sea.

By integrating the information from the well and performing direct hydrocarbon indicator analysis, the zone of interest was defined. Extended elastic impedance analysis was performed to determine the optimal angles corresponding to fluid and lithology projection. The optimal angles chosen from the well logs do not necessarily represent the optimal angles in the seismic, but give a good insight of the properties of interest and fine tuning is required. Scaled reflectivities at the respective χ angles were produced. The fluid and lithology cubes were produced $\chi = 20^0$ and $\chi = -50^0$ respectively.

A coloured inversion operator was designed from the wells available. The operator re-shapes the amplitude spectra of the seismic to the well and hence earth's amplitude spectrum within the band limits of the spectrum In addition to the amplitude re-shaping a -90 phase rotation was applied as part of the inversion algorithm. The scaled reflectivities were convolved with the coloured inversion operator, resulting in band limited impedances.

Seismic net pay estimation was performed on the band limited impedance of the fluid projection with the assumption that the average band limited impedance within the zone of estimation is proportional to the net if the tuning effect is removed. A simple wedge model is used in obtaining a detuning function to eliminate the tuning effect, boosting the average band limited impedance in the thicker parts. Seismic calibration aimed at associating the average band limited impedance with the seismic net-to-gross was also applied. Due to the lack of adequate well data, well calibration was not performed. The algorithm can be used to estimate net-pay for reservoir thicknesses above the tuning thickness depending on the lower frequency component in the seismic data.

The work flow has been found useful and can be particularly important in areas where there is limited data.

ACKNOWLEDGMENTS

TABLE OF CONTENTS

LIST OF TABLES AND FIGURES

LIST OF ABREVIATIONS

ρ	Density
VP	P wave velocity
VS	S wave velocity
ΔVS	Contrast in S wave velocity of layers
ΔVP	Contrast in P wave velocity of layers
VS0	Average S wave velocity of layers
VP0	Average P wave velocity of layers
K	Ratio of S-wave velocity to P-wave velocity
Z, AI	Acoustic Impedance
θ	Angle of incident
$Z(\theta)$	Elastic Impedance
χ	Chi
$Z(\chi)$, EEI	Extended Elastic Impedance
R0	Normal incidence reflection coefficient
RSc	Scaled reflectivity
A	AVO intercept
B	AVO gradient
C	Curvature
TWT	Two Way Time
FFT	Fast Fourier Transform
IFFT	Inverse Fast Fourier Transform
AVO	Angle Versus Offset
PHIT	Total porosity
Sw	Water saturation
Vshale	Shale volume fraction
BLI	Band limited impedance

1. INTRODUCTION

Traditionally seismic has been used to describe geological structures and it provides the means to interpret the subsurface structural framework and build geological models, which are crucial in the oil and gas industry. In the past few decades advancements in geophysical technologies based on continuous research have significantly increased the scope of application of seismic data from conventional structural mapping to more advanced definition and characterization of reservoir. At the same time the role of seismic methods has evolved from being a tool in exploration and development of discoveries to full range reservoir characterization and field management. The reliability of seismic data and various amplitude analysis methods has greatly reduced the risk associated with drilling wells in existing fields, and the ability to add geophysical attributes and constraints to statistical models has provided a mechanism for directly delivering geophysical results to the reservoir geologists and engineer (Pennington, 2001). In the sense of reservoir characterization it has been used to provide estimates of reservoir properties such as porosity and net-to-gross. The procedure of determining the reservoir properties with the application of seismic methods is referred to as seismic reservoir characterization. The focus of this thesis work will be on the application of modern seismic tool for reservoir characterization in the Norwegian Sea.

Objective: The robust workflows for seismic reservoir characterization proposed by Connolly (2010) will be particularly implemented so as to test applicability of the work flow.

The seismic characterization method will be implemented in an area from the Norwegian Sea. The study area is a deep water horizon where data availability is limited and exploration activities are risky. It is therefore important that we use the available seismic data in the reservoir characterization.

2. THEORETICAL BACKGROUND

This chapter deals with the explanation of the theoretical background of the techniques which are going to be employed in this work. The workflow to be applied mainly contains three steps, namely extended elastic impedance (EEI) analysis, coloured inversion and net pay estimation. The principles behind each step will be presented based on the order of the implementation.

2.1 Extended elastic impedance

The contrast of material properties at an interface between different layers, where the reflection takes place, is a very important factor that controls the strength of reflection at a subsurface interface. It is the basis for the different types of seismic amplitude analysis. The relationship between the seismic reflections and hence amplitudes to the properties of the subsurface materials can provide the means to predict the petrophysical and reservoir properties. In order to work with petrophysical and reservoir properties, we need to work in the impedance domain which reflect the material (lithology) property rather than the reflectivity domain which describes the property contrast at the interface between different lithologies. In this respect the most commonly used property is the acoustic impedance (Z), the product of rock density (ρ) and *P*-wave velocity (V_p). The reflection coefficient at the interface between two layers depends on the acoustic impedance of the layer above and below it. The reflection coefficient for normal incident angle is given by,

$$R_0 = \frac{Z_{i+1} - Z_i}{Z_{i+1} + Z_i} \; ,$$
[2.1]

where, Z_{i+1} and Z_i are acoustic impedances of the layers above and below the interface.

The reflection coefficient for non-normal incident angle is a function of incident angle in addition to the impedances and is described by the Zoeppritz (1919) equation. The Zoeppritz equations are complicated but there are simpler and very useful approximations of the equations by Bortfield (1961), Aki and Richards (1981) and others. Aki and Richards (1981) defined the reflection coefficient using three terms involving P-wave velocity, S-wave velocity and density based on the assumption of weak contrast of the parameters as compared to the average of the respective parameters. Shuey (1985) rearranged the Aki and Richards (1981) linearization equation in terms of the intercept (A), gradient (B), and curvature (C) as

$$R(\theta) = A + B\sin^2\theta + C\sin^2\theta\tan^2\theta, \qquad\qquad [2.2]$$

where,

$$A = \frac{1}{2}\left(\frac{\Delta V_P}{V_P} + \frac{\Delta\rho}{\rho}\right), \qquad\qquad [2.3]$$

$$B = \frac{1}{2}\frac{\Delta V_P}{V_P} - 4\frac{V_S^2}{V_P^2}\frac{\Delta V_S}{V_S} - 2\frac{V_S^2}{V_P^2}\frac{\Delta\rho}{\rho}, \qquad\qquad [2.4]$$

$$C = \frac{1}{2}\frac{\Delta V_p}{V_p}. \qquad\qquad [2.5]$$

ΔV_P, ΔV_S and $\Delta\rho$ are the contrasts in the P wave velocity, S wave velocity and density,

V_P, V_S and ρ are the averages of P wave velocity, S wave velocity and density of the layers above and below the interface.

The angle θ is the angle of incident and more precisely it is determined as the average of the incidence and transmission angles at a plane reflecting interface. For incidence angles between less than 30^0, the third term involving C can be neglected and the two terms left can provide reasonable approximation.

The normal incidence reflection coefficient, defined by the contrast of acoustic impedance, can sufficiently represent the reflection coefficient for smaller reflection angles as the reflection coefficient changes slowly for angles of incidences close to the zero. Accordingly, acoustic impedance has been used in seismic inversion and calibration of zero offset data. It can't, however, be used in similar manner for reflection coefficients at larger angles of reflections. Connolly (1999) generalized acoustic impedance for non-normal incidence angles and defined the elastic impedance to allow the benefits of inversion to be exploited for AVO data. He defined the elastic impedance as a function, $Z(\theta)_i$, which has properties analogous to the acoustic impedance and represented the reflection coefficient at an incident angle, θ, in the form

$$R(\theta) = \frac{Z(\theta)_{i+1} - Z(\theta)_i}{Z(\theta)_{i+1} + Z(\theta)_i}. \qquad\qquad [2.6]$$

The elastic impedance is derived from Shuey's (1985) linearization equations as a function of θ, P wave velocity (α), S wave velocity (β) and density (ρ) as

$$Z(\theta) = V_P^{1+\sin^2\theta} V_S^{-8K\sin^2\theta} \rho^{1-4K\sin^2\theta}, \qquad [2.7]$$

where, $K = (V_S/V_P)^2$.

The expression, K, is constant and is computed over the interval of interest on the log. The elastic impedance provides a consistent framework to calibrate and invert nonzero-offset seismic data just as AI does for zero-offset data and is dependent on P and S eave velocities and density (Connolly, 1999). The elastic impedance was later normalized by Whitcombe (2002A) in such a way that its variable dimensionality and significant changes in the resulting numerical values with θ are avoided by providing an elastic impedance function (equation [2.8]) which returns normalized impedance values for all angles. The normalizing parameters used are V_{P0}, V_{S0}, ρ_0 are the average P wave velocity, S wave velocity and density respectively and result in

$$Z(\theta) = V_{P0}\rho_0 \left[\left(\frac{V_P}{V_{Po}}\right)^{1+\sin^2\theta} \left(\frac{V_S}{V_{So}}\right)^{-8K\sin^2\theta} \left(\frac{\rho}{\rho_o}\right)^{1-4K\sin^2\theta} \right]. \qquad [2.8]$$

The two-term AVO linearization defines a straight line for reflectivity against $\sin^2\theta$ (Figure 2-1). One can determine the AVO parameters A and B from intercept and gradient of the straight line respectively with the angles of incidence in the range between 0^0 and 30^0 and build reflectivity for any $\sin^2\theta$ as a weighted sum of intercept and gradient using the two term AVO linearization. The use of elastic impedance for this purpose poses two limitations related to the need for $\sin^2\theta$ to exceed unity and possibility of getting correlation coefficient values beyond unity (±1). If we extend the line (Figure 2-1) beyond the linear fit we observe that

 a) The linearization approximates physically reality between 0^0 and 30^0($\sin^2\theta$=0.25),
 b) $\sin^2\theta$ values between 0 and 1 have corresponding angle, θ
 c) $\sin^2\theta$ values less than zero and greater than unity can't have equivalent real angle
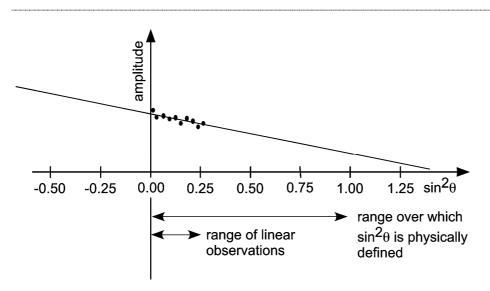
Figure 2-1 Pre-stack amplitude observations are fit with the two-term AVO linearization (Whitcombe, et al., 2002).

Whitcombe et al., (2002) modified the definition of elastic impedance beyond the range of physically meaningful angles by substituting $\tan \chi$ for $\sin^2\theta$ in the two-term reflectivity equation and provided a scaled version of reflectivity (R_{SC}) to be normal reflectivity multiplied by $\cos\chi$, which ensures that reflectivity don't exceeds unity. The scaled reflectivity is given as,

$$R_{SC}(\chi) = A\cos(\chi) + B\sin(\chi) \quad . \qquad\qquad [2.9]$$

The extended elastic impedance (EEI) is given as

$$Z(\chi) = V_{P0}\rho_0 \left[\left(\frac{V_P}{V_{Po}}\right)^{\cos(\chi)+\sin(\chi)} \left(\frac{V_S}{V_{So}}\right)^{-8K\sin\chi} \left(\frac{\rho}{\rho_o}\right)^{\cos(\chi)-4K\sin\chi}\right]. \quad [2.10]$$

We note that the EEI is not a function of angle of incidence, but of χ. The scaled reflectivity have two end points the AVO intercept at $\chi = 0^0$ and AVO gradient at $\chi = 90^0$. While the EEI reflectivity at $\chi = 0^0$ is acoustic impedance (denoted AI from this point forward), the EEI reflectivity at $\chi = 90^0$ is gradient impedance (GI) as referred by Whitcombe et al. 2002. The GI can be derived from equation [2.10] by setting $\chi = 90^0$ resulting in

$$GI = V_{P0}\rho_0 \left[\left(\frac{V_P}{V_{po}}\right)^1 \left(\frac{V_S}{V_{So}}\right)^{-8K} \left(\frac{\rho}{\rho_o}\right)^{-4K}\right]. \qquad\qquad [2.11]$$

Acoustic impedance (AI) is a function of P wave velocity, V_P, and the density, ρ, while the gradient impedance (GI) is a function of S wave velocity, V_S as well. AI and GI can be cross plotted to define the impedance form of the AVO intercept versus gradient reflectivity cross plot (Whitcombe et al., 2001). By defining $AI_0 = V_{P0}\rho_0$, EEI can be rewritten in terms of AI and GI, where the angle χ represents the coordinate rotation angle within the AI-GI domain as

$$Z(\chi) = AI_0 \left[\left(\frac{AI}{AI_o} \right)^{\cos(\chi)} \left(\frac{GI}{AI_o} \right)^{\sin(\chi)} \right]. \qquad [2.12]$$

The log-log AI-GI cross plot (figure 2-2) can be used to define the rotation angle, χ, enabling the production of EEI logs that can reasonably approximate the different elastic parameters (κ, λ, V_p/V_S and μ in Whitcombe et al., 2002) and reservoir properties (Vshale , Sw, PHIT in Arslan and Yadar, 2009). Since the impedance logs are multiplied [equation 2.12] the combination of the logs in a coordinate rotation must be operated in log-log space as

$$Z(\chi) = \ln(AI)\cos(\chi) + \ln(GI)\sin(\chi). \qquad [1.13]$$

We shall also remember that the normal incidence reflectivity function can be expressed in terms of the differentiation of the natural logarithm of impedance function. The appropriate χ value, that produces the optimal EEI logs defining the target property/parameter, can be decided based on the correlation coefficient between EEI logs and the well logs. Whitcombe et al. (2002) showed that EEI can be used in fluid or lithology prediction.
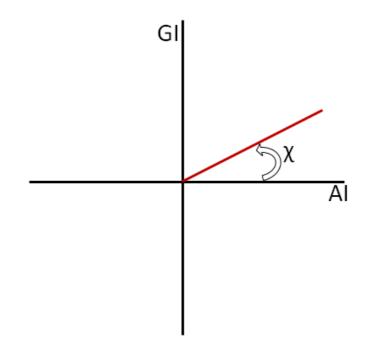
Figure 2-2 AI-GI cross plot

2.2 Coloured Inversion

Seismic inversion is a powerful methodology to predict the rock properties from the reflection seismic data set. It allows better understanding of the reservoir as it inverts reflectivity at the interface to layer properties. There are several methods of inversion to invert the reflection seismic data to impedance data. An attempt to obtain absolute acoustic impedances comparable to the impedance acquired from well can be considered absolute acoustic impedance inversion and requires the addition of background impedance data. In contrast some algorithms transform seismic reflection to relative impedance values and may be considered as showing the apparent band limited acoustic impedance contrasts. The term 'band limited' is related to the fact that the seismic data we use is limited to certain frequency levels and lack low and high frequencies. The inversion algorithm used for this study is the coloured inversion (Lancaster & Whitcombe, 2000), a simple and fast technique to invert band-limited seismic data to relative impedance.

Inversion of the band limited seismic to band limited impedance requires the proper understanding of the characteristics of the impedance amplitude spectra. It has been observed that earth's geological features, follow a power law distribution and fractal geometries (Talling, 2001). The power law distribution have the property that when plotted in log-log appears to have strong linear relationship of the form f^{α}, where α is the power law exponent. We can observe a strong negative linear relationship with a negative power law exponent in a log-log plot of amplitude versus frequency for a Fourier transformed well log (Figure 2-3). This nature reflects the biasness of earth's spectra to low frequency. This concept can be used in reshaping the amplitude spectrum of the seismic data, so that it resembles the earth's amplitude spectra within the band limits of the frequency of the seismic. It is the main objective of the coloured inversion algorithm and can be achieved by designing an operator which reshapes the spectrum and apply -90^{0} phase rotation in order to invert the seismic in to impedance form. The reshaping is achieved by determining the power law coefficient, α, which can be estimated by curve fitting from the well logs in an amplitude versus the frequency plot (log - log).

Figure 2-3 shows a depth to time converted acoustic impedance log (left) and the frequency versus amplitude log-log plot. The slop of the trend line (red) is used to design an operator that reshapes the seismic amplitude spectrum.

The coloured inversion is analogous to trace integration except that the amplitude reshaping is based on the real earth amplitude spectrum. The need and effect the -90^0 phase rotation in the coloured inversion can be explained by studying trace integration of harmonic signals. Trace integration of harmonic signals gives,

$$Z(t) = Z(0)\exp\left[\int_0^t R(t)dt\right] = -i\frac{A}{\omega}exp[i\omega t]. \qquad [2.14]$$

The $-i$ term in the right hand side of equation represents the -90^0 phase rotation required to transform the trough and peaks to zero crossings so that the zero crossings would represent the top or base of a layer.

The coloured inversion as the trace integration doesn't involve the addition of low frequency data which is required to achieve seismic inversion to absolute impedance.
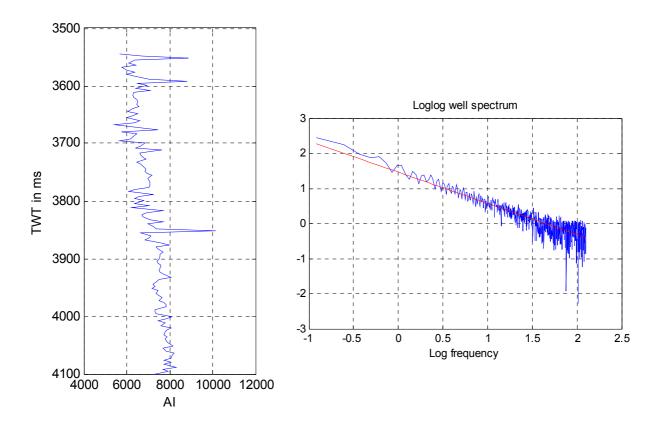

Figure 2-3 Acoustic impedance log in time and its log-log amplitude spectrum

2.3 Net-to-gross

Net-to-gross is one of the main parameters in reservoir characterization and can be defined as the ratio of the value of an average measurement, such as gamma ray, across the reservoir to the value of that measurement for the 100% net case (Connoly, 2010). It represents the part of the reservoir which can produce hydrocarbon relative to the case where the gross reservoir thickness is producing. The need for the determination of net-to gross arise from the fact that common reservoirs don't have uniform producing sand composition rather also contains some proportion of shale or non-reservoir lithology. Determination of the net-to-gross from seismic can be useful given the extensive lateral coverage it possesses compared to the well logs, hence a number of work have been conducted. Early net pay estimation methods were based on the trough and peak amplitude measurements corresponding to the top and base of the reservoir. The amplitude at the top and bottom of the gas saturated reservoir can be an indicator of the presence of hydrocarbon. These amplitudes are affected by the changing thickness of the reservoir. Determining amplitude in the reservoir can be complicated due to the interference of reflections. The interference effects related to the top and bottom of a sand reservoir with shale above and below it can be investigated by observing the thickness in a simple wedge model (Figure 2-4, A, B). The trough and peak amplitudes at the top and base of thick layer correspond exactly to reflection coefficients. However, for thinner layers the amplitude depends on the nature of interference i.e. constructive or destructive and this is commonly referred to as the tuning effect. The amplitude increases when constructive interference exist and decrease to minimum when destructive interferences exist.

The tuning curve (Figure 2-4 C, D) which can be determined in a cross plot of seismic thickness versus the composite amplitude at the peak and through can be used to understand how the amplitude varies with respect to the changing apparent thickness. The shape of the tuning curve is dependent on the wavelet. The maximum point in the amplitude tuning curve represents the amplitude at wedge thickness below which the peak and trough separation remains constant (Simm, 2009). This thickness is commonly referred to as tuning thickness and below it the amplitude decrease in response to the thinning thickness. Neff (1977) and Schramm et al., (1977) among others conducted modeling of thin reservoir with thickness less than the tuning with varying thickness of sand and shale and concluded that for thin zones the composite amplitude is roughly linear with changing net thickness of sand in simple reflection models. This relationship was used as a basis for determining the net pay for thin reservoir zones. Brown (1984), proposed a method to estimate net pay based on the similarity of the

data cloud outline on the crossplot of composite amplitude versus seismic thickness and the simple single-layer tuning curve derived knowing the wavelet in the data (Simm, 2009). Amplitude scaling techniques to remove the tuning effect were employed to estimate the net pay from the corrected amplitudes. As the thickness increases the reliability of this method diminishes as the amplitude is increasingly biased on the rock property contrasts.
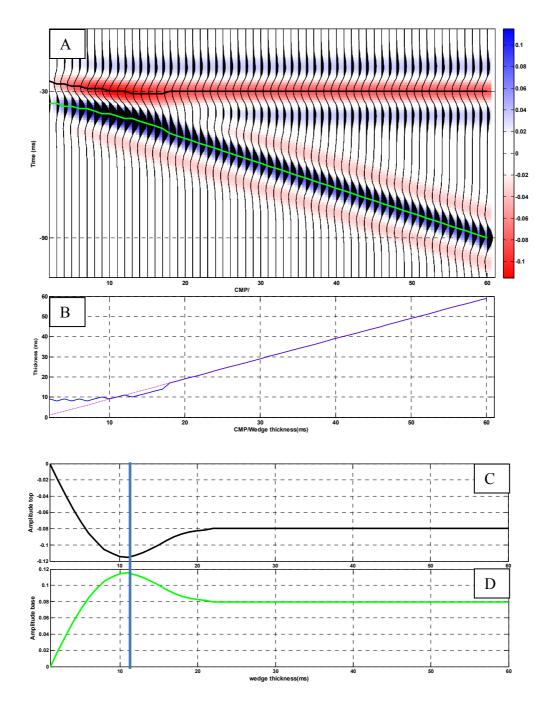

Figure 2-4 Simple seismic reflection wedge model (A), wedge thickness versus pick thickness (B) and the tuning curves for model at the base (D) and top (C) of the wedge. Red colour represents negative amplitude and blue represents positive amplitude. The blue line indicates the tuning thickness.

Another approach to estimate the net pay is based on band limited impedance. Connolly (2007) proposed a net pay estimation algorithm that is comprised of detuning of the tuning effect and calibration for the net pay estimations. The algorithm uses the assumption that the integral average band limited impedance between two seismic picks picked at the zero crossings is proportional to the net pay if the response of the gross interval is detuned.

A simple band limited impedance wedge model (Figure 2-5, A) is used in the detuning process assuming that the wedge model represents the reservoir being modeled. As the thickness decreases the apparent thickness decreases as well, but the average band limited impedance (BLI) exhibit the tuning pattern. The tuning curve (Figure 2-5, B, C) defined by cross plotting the expected band limited impedance with the time separation between the top and base of the wedge which is referred to as apparent thickness is used to detune the tuning effect present in the seismic data. Since the curve is sensitive to the wavelet embedded in the wedge, one must construct the tuning wedge using the same wavelet as the one embedded in the seismic data to ensure proper detuning. Determining the net pay thickness within the apparent thickness rather than the true gross thickness can be achieved by knowing the ratio between the net pay and apparent thickness referred to as seismic net-to-gross (Connolly, 2007). The seismic net-to-gross will be equal to the true net-to-gross for large gross thickness but decrease rapidly for smaller thickness as the apparent thickness geos to the minimum level. The tuning and seismic net-to-gross curves (Figure 2-5, D) can be used to derive the detuning transform function.

The core assumptions in this method are the average of the band limited impedance over the apparent thickness is proportional to seismic net-to-gross for a fixed apparent thickness and that this dependence on apparent thickness can be removed using the detuning function (Connolly, 2007). Once the tuning effect corrected, the tuning curve has to be calibrated against the seismic impedance data so that the impedance values are correlated to the seismic net-to-gross. Seismic calibration can be iteratively applied by assigning a correction factor such that impedance values will be enveloped by the tuning curve. Depending on the availability of adequate calibration data and the depth range of the reservoir, a depth dependent (spatially variant) or a constant calibration factor can be used (Connolly, 2007). If well data exists the seismic net-to-gross can be calibrated with the actual net to gross values determined petrophysical analysis from wells.
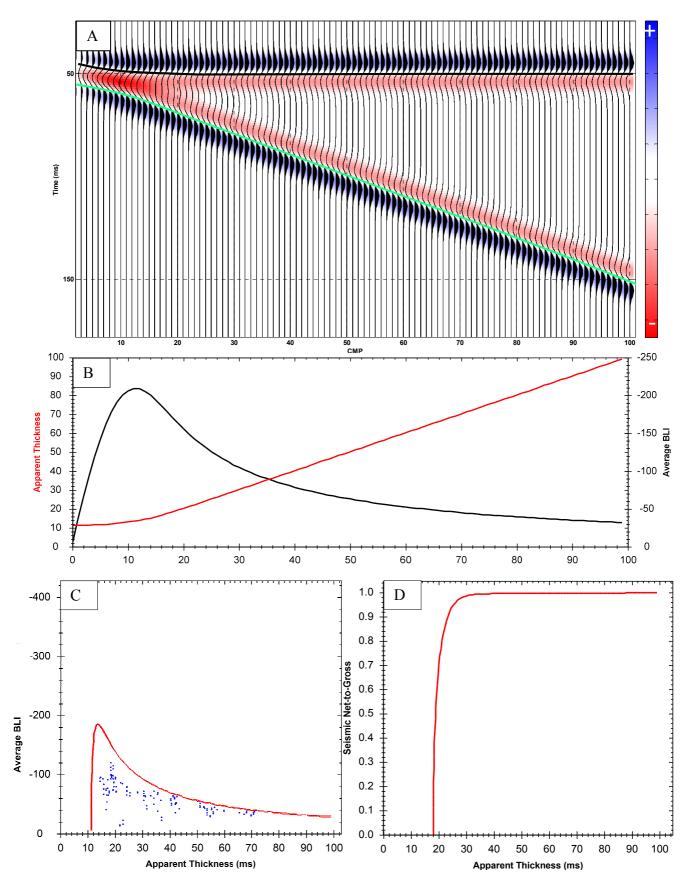
Figure 2-5 Band limited impedance wedge model (A) and the apparent thickness and average band limited impedance (BLI) between the top and base the wedge (B). (C) Tuning curve and (D) seismic net-to-gross

3. SEISMIC AND WELL LOG DATA

In this chapter a brief geological and geophysical description of the area from which the data set was takes is provided. First short regional sub regional explanation is provided. It is followed by the geophysical description about the preparation of the data for analysis. The data used for the implementation of the seismic characterization work flow is from the western margin of the Norwegian Sea. Brief geological setting of the study is presented based on previous works.

The area is located in the Vøring basin which is deep water passive margin basin located offshore central Norway. Vøring Basin area has been subjected to several tectonic episodes since the Caledonian orogeny in Ordovician–Silurian times (Brekke et al,. 1999, Ritter et al., 2004). Several uplifted structures such as the Gjallar and Nyk (Figure 3-1) have been important in shaping the sedimentological pattern of the basin. The tectono-stratigraphic framework from the Upper Jurassic to the Eocene secession in the Norwegian Sea is displayed in Figure 3-2 (Lien, 2005). It is composed of the main exploration target formations such as the Tang, Springar, Nise and Kvitnos. Turbidite sheets and submarine sandstones interbedded with shale are the main reservoir rocks. Maastrichtian Springar formation is present in the studied area.

The 500 Km^2 3D dataset is taken from the Gjallar ridge area. The near, mid and far offset partial stacks with 3-15^0, 13-25^0 and 23-35^0 respectively were provided by WesternGeco. Well log data for the two wells existing within the extent of the seismic data set were was provided by Statoil ASA.

Seismic well tie procedure has been performed to establish the link between the seismic reflections and stratigraphy with the aid of the wells available in the area. Furthermore, synthetic seismogram showing the expected seismic response for comparison with the real seismic data was generated (Figure 3-3). This was helpful in identifying and correlating the zones of interest depicted from the well to the seismic data. The time-depth relationship required to make the synthetic seismogram is established from the check shots.

The seismic well tie revealed that the top of the reservoir corresponds to the strong reflector in a trough in a normal polarity, while the base of the reservoir corresponds to a peak. This is consistent in the two synthetic seismograms formed from the two existing wells.
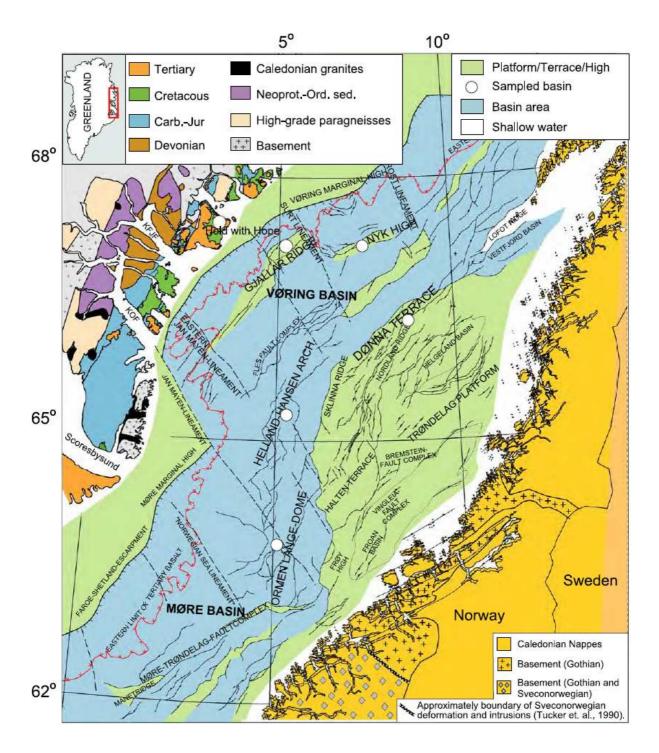
Figure 3-1 Structural elements of the platforms and basins within the Norwegian Sea and simplified geological maps of the conjugate margins of the East Greenland and Norway (Fonneland et al 2003).
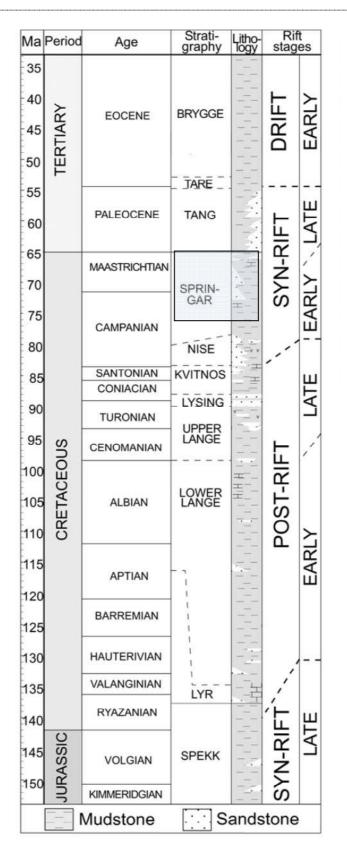
Figure 3-2 Tectono-stratigraphic framework of the Upper Jurassic to Eocene succession for the Norwegian Sea region (Lien 2005). The reservoir zone of interest for this work is marked.
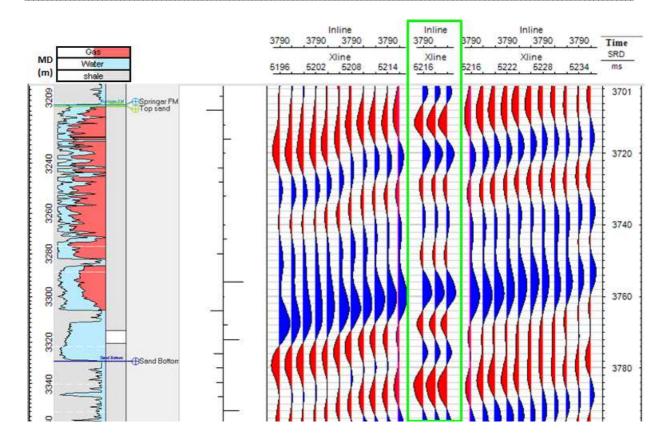
Figure 3-3 Seismic well tie and synthetic seismogram (in green box)

4. METHODOLOGY

The principles and theoretical background behind the methodology used in this work are presented in chapter 2. The detailed methodology in each step will be described in this chapter and references to the previous chapter are provided where necessary.

The workflow (figure 4.1) to be implemented is composed of mainly three steps, (1) Extended Elastic Impedance analysis (2) coloured inversion and (3) net-pay calculation and are applied consecutively.
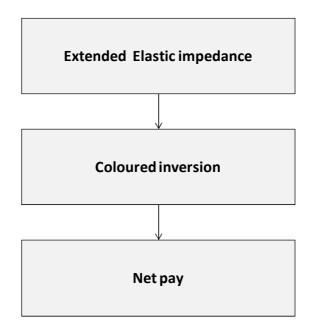
Figure 4-1 Simplified work flow for net pay estimation

4.1 Data quality requirement for extended elastic impedance and coloured inversion

To determine the elastic parameters and reservoir properties 3D seismic data and good quality wire line logs are required. The pre-stack seismic data should be migrated and corrected for noise. Good quality wire line logs are required to determine the optimal χ angle and are vital to the successful application of the technique.

4.2 Petrophysical analysis

Petrophysical analysis is conducted to determine the various reservoir properties, which are valuable in determining the presence and quantity of hydrocarbon. The full analyzed logs including Gassmann (1951) substitution was provided by Statoil.

4.3 Extended Elastic Impedance

The extended elastic impedance analysis involves

- the calculation of EEI logs from P wave velocity, S-wave velocity and density logs,
- determination of optimal χ angle,
- estimation of the amplitude versus offset (AVO) parameters intercept (A) and gradient (B) from partial stack seismic data,
- production of scaled reflectivity volumes that represent the petrophysical or reservoir property of interest.

The EEI logs can be calculated from P-wave velocity, S-wave velocity and density logs by using equation [1.10] for χ angle ranges of -90^0 to 90^0. The EEI logs with χ angles 180^0 apart will have associated reflectivity series with opposite polarity; hence the correlation is performed with in a range of 180 degrees. The petrophysical logs of interest can be correlated to EEI logs to decide the optimal angle representing the desired petrophysical property. The χ angle with the maximum correlation coefficient is considered to be the optimal angle. Since rock properties change with depth and the optimal chi angle is likely to change with depth, log interval at which the correlation takes place was carefully decided. The analysis was conducted in the intervals of interest (3200 – 3400 m), which significantly improves the correlation between EEI and log well log derived properties result in better optimal angle.

Two petrophysical logs namely volume fraction of shale (VShale) and water saturation (Sw) for the well located in the area of interest have been correlated with the EEI logs to determine the optimal χ angles. In Figure 4-2, the correlation coefficients are plotted against the χ angles and the maximum correlation coefficients for the petrophysical properties of interest and the optimal χ angles presented in Table 4-1.
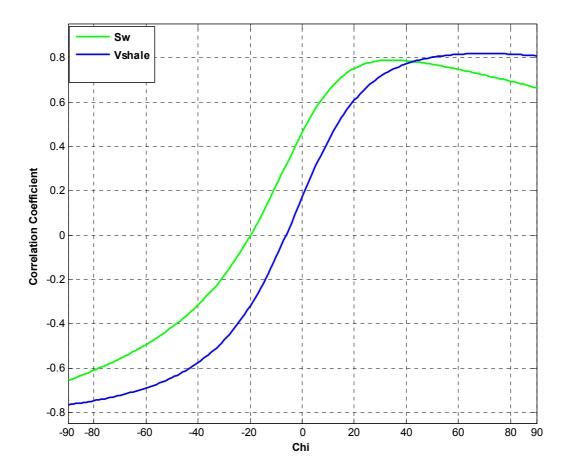
Figure 4-2 Correlation coefficient for Vshale (green), Porosity (PHIT, red) and SW (blue)

Parameter	Correlation Coefficient	χ
Vshale	0.82	70
Sw	0.79	34

Table 4-1 Maximum correlation values and the corresponding optimal angle (χ) for Vshale, and Sw for one of the wells.

The extended elastic impedance derived and the corresponding petrophysicaly derived logs are presented in Figure 4-3. As the correlation indicates, a higher similarity is observed in Vshale logs while minimal similarity is observed in the total porosity.

Figure 4-3 EEI derived logs (black) of Vshale and Sw and the corresponding petrophysically derived well logs (blue)

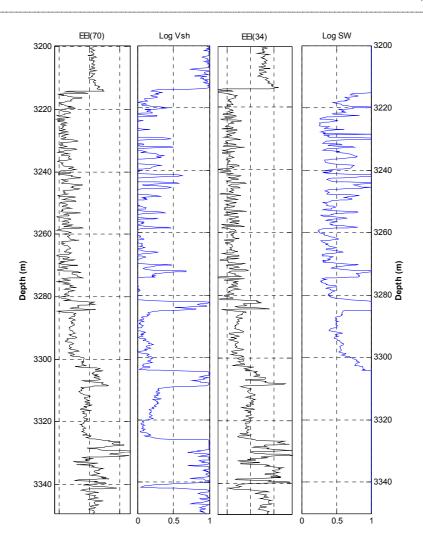Alternatively, the EEI logs can be calculated by considering χ as an angle of rotation in the AI-GI cross in the log-log domain. This requires the calculating the gradient impedance (GI) at $\chi=90^0$ from equation [2.11]. Given the acoustic and gradient impedance logs, the EEI logs can be calculated using equation [2.12]. The optimal angle is decided by rotating angle of projection until a rotation angle that discriminate the different classes such as facies classes of sand and shale.

Once the optimal angles are determined the EEI reflectivities of desired petrophysical properties can be produced from equation [2.9]. This requires the determination of AVO parameters A (Intercept) and B (Gradient). The two AVO parameters are derived by simple linear fit from the reflectivity versus $\sin^2\theta$, where θ is a representative angle from the near, mid and far offset partial stack (Figure 4-4) and A and B (Figure 4-5) are the intercept and slope (gradient) of the line respectively.
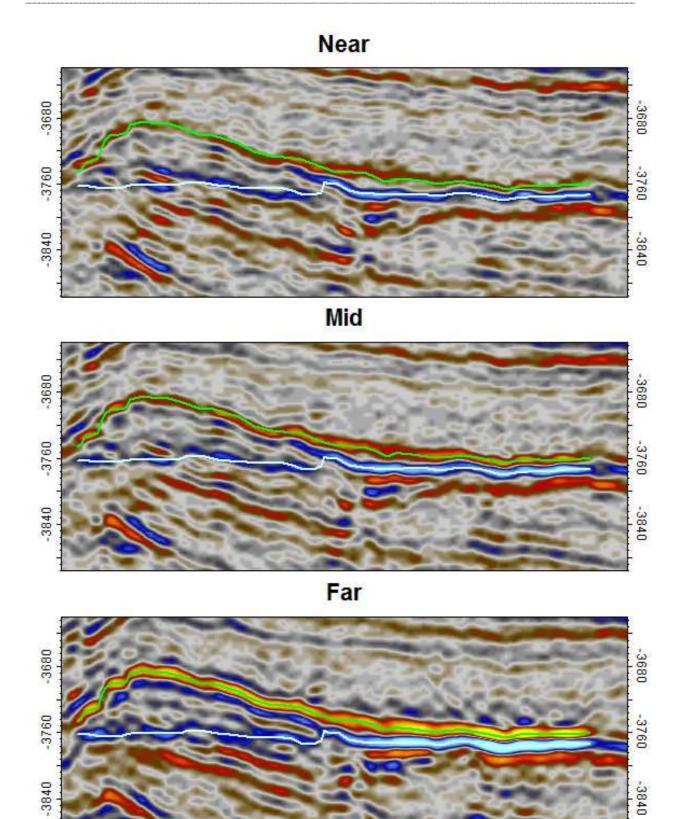
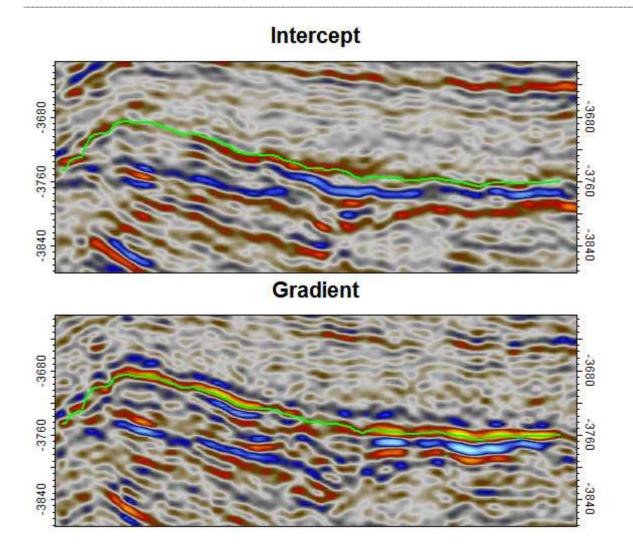Figure 4-4 Near, mid, and far offset stacks (top to bottom, left)

Figure 4-5 The AVO Intercept (top) and Gradient (bottom) (right) estimated from the partial stacks

The scaled reflectivities are then produced as weighted sum of intercept (A) and gradient (B). These reflectivities are input to the coloured inversion, which is the next step in the net pay estimation steps.

Fluid and lithology cubes

To image the reservoir, scaled reflectivity at the fluid projection angle has been produced. This results in a fluid cube and it was used as a base to estimate the net pay. The optimal fluid projection angle χ was interactively determined by varying χ angle and $\chi= 20^{0}$ highlight the gas-water-contact and define the gas filled reservoir from the brine field part of the reservoir. Similarly a lithology projection angle was determined and the lithology cube was made at the $\chi= -50^{0}$. The lithology cube highlights the lithology contacts between the sand and shale.

4.4 Coloured Inversion

Adjustment of the seismic spectrum to power law spectrum of the earth within the band-limits of the seismic is the main objective of the coloured inversion (CI). The input to the CI should be zero phase. If it is not, phase rotation of the inverted data by comparison with the AI logs is required. The determination of power law exponent (α) is required to make a coloured inversion operator with -90^0 phase shift, whose amplitude spectrum maps the mean seismic spectrum to the mean earth AI spectrum (Lancaster & Whitcombe, 2000). The gross spectral form of logs from wells in any given field is reasonably constant; it is therefore adequate to perform the inversion using a single convolution operator. The design of the operator is described below.

4.4.1 *Determining well log amplitude spectrum.*

Designing the operator requires the determination of amplitude spectrum for the well logs. This can be achieved by applying Fast Fourier Transform (FFT) to the time converted impedance logs. A time converted acoustic impedance log has been used for the derivation of the operator. The data was resampled at 4ms, which can sufficiently represent the frequencies up to 125 Hz. The log impedance versus frequency log- log plot allows the determination of the gradient, alpha (α), which will be used to map the seismic spectrum to a curve of the form f^α (Lancaster & Whitcombe, 2000). The calculated alpha values for the two wells are very close i.e. 0.84 and 0.81, which suggest the alpha value with in the area is reasonably constant.

4.4.2 *Band pass filter*

Coloured inversion is a band limited inversion technique and hence we apply a Butterworth band pass filter with minimum and maximum frequencies of 8 and 75 Hz respectively to band limit the impedance log spectrum within the seismic band width. This band limited impedance spectrum can now be used to design an operator that can be used to shape the seismic amplitude spectrum to that of the log spectrum (Figure 4-6).
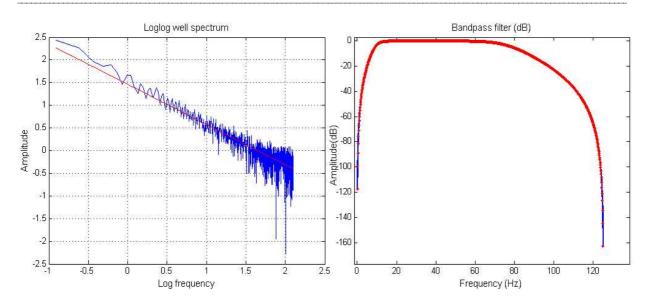
Figure 4-6.The log-log amplitude spectrum of the AI log with best fit line (red line) and the band pass filtered impedance log (right)

4.4.3   Seismic amplitude spectrum

The mean amplitude spectrum of the seismic amplitude spectrum is then derived from the seismic data. To be used in the design of the operator the mean spectrum is smoothed (Figure 4-7). The smoothed seismic mean spectrum can now be mapped to match the band pass filtered log spectrum by subtracting it from the log spectrum. A phase rotation of -90^0 has been applied to the operator. The -90 phase shift is in line with the requirement that the inversion is applied to transform zero phase seismic (reflection) to impedances. Moreover, the use of 90° phase is helpful in thin-bed interpretation because it eradicates the dual polarity of the thin-bed response allowing for improved imaging of thin-bed geometry, impedance profiles, and lithology (Zeng & Backus, 2005). The operator in the frequency and time domain, produced by the Inverse Fast Fourier Transform (IFFT) algorithm, are shown in Figure 4-8. The designed operator is used to convolve the desired seismic dataset in such a way that the amplitude spectrum is matched with the spectrum of the earth, which is recorded in the impedance log. The inversion can be performed both in the time as well as in the Fourier domain.
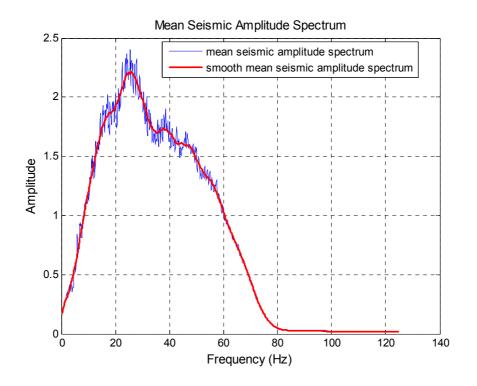
Figure 4-7 Mean (blue) and smoothed (red) amplitude spectrum of the seismic data
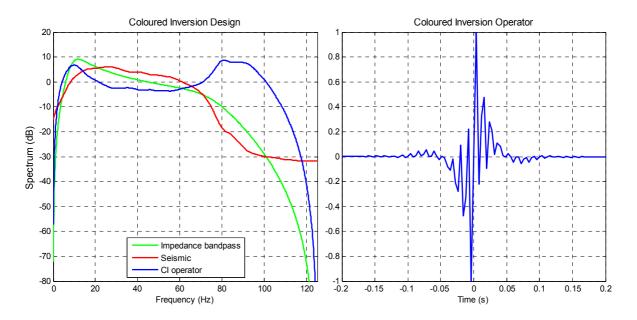

Figure 4-8 The coloured inversion operator in the frequency and time domains

4.5 Net-to-gross

The objective for this algorithm is to estimate the total net pay between two seismic picks made on zero-crossings of band-limited impedance data. The band limited impedance was produced by applying the colour inversion to EEI reflectivity that differentiate pay and not

pay. To ensure that the impedance is a single hydrocarbon phase, which is one of the requirements for successful application of the algorithm, the base was picked at the gas-water-contact. The fluid cube was used as the base for the net pay estimation.

A wavelet representing the input seismic data is required to build the impedance wedge model and hence the tuning curve. The wavelet extracted was complicated and the estimations attempts were not successful. Hence, to ensure the band limited nature of the wedge mode, a 8-10-50- 75 Hz band pass filter, which is equivalent to the band pass filter applied during the generation of the colour impedance operator is used to build the impedance wedge model Figure 4-10. The lower frequency component governs the maximum apparent thickness that can be effectively measured. As a rule of thumb the thickness should not exceed the half cycle of the lower frequency component in the data. Hence, with 8Hz frequency it could be possible efficiently estimate the net pay for thickness within 60ms.

The reservoir zone is determined based on the preceding steps and hence the top and base of the reservoir zone are picked for the estimation. The algorithm is sensitive to the location of the pick hence, automatic snapping (Figure 4-9) to the zero crossings was applied to ensure exact pick. Once the top and base of the reservoir are picked, the two basic attributes, the apparent time thickness and the average band-limited impedance between the picks were derived. The attributes are then cross plotted and superimposed with the tuning curve determined from the impedance wedge model. From the discussion provided in the theoretical back ground, it is recalled that that the points on the tuning curve (Figure 4-11) have a net-to-gross of 1 while those on the x-axis have 0 net-to-gross. The points in between are scaled linearly between 0 and 1.

Net pay is defined by the product of net-to-gross and the gross thickness of the reservoir and we can modify this to determine the seismic net-to-gross (N_S) by using apparent thickness (T) instead of the gross thickness. Hence, the net pay thickness (P) can be determined easily if we know the apparent thickness as

$$P = N_s T \quad .$$ [4.1]

The seismic net-to-gross (Figure 4-12) which is defined as the ratio between the true and apparent thickness of the wedge model and decreases dramatically at lower apparent thickness. Recalling the key assumption that the seismic net-to-gross is proportional to the

average band limited impedance, a detuning correction (Simm, 2009) (Figure 4-13) can be defined as

$$S = \frac{N_S}{\overline{Z_S}},$$ [4.2]

where $\overline{Z_s}$ is average band limited impedance. Substituting equation [4.2] in equation [4.1] we get

$$P = S\overline{Z_s}T.$$ [4.3]

As we can observe in the Figure 4-13, the detuning correction increases with apparent thickness and it effectively boosts the impedance for higher apparent thickness.

Once the detuning is performed using the band limited impedance wedge, seismic and well calibrations are needed to change the band limited impedance values to seismic net-to-gross. The seismic calibration was performed by manually adjusting tuning curve in such a way that it will envelop the data points. The calibration amplitude (light blue curve in Figure 4-11), inverse of the detuning correction, helps in appreciating the nature of scaling in predicting net pay (Simm, 2009). Data points on this line have net-to-gross value of one and those in the x-axis will have 0 net to gross. Since only one of the wells is located within the limits of the estimation zone, well calibration was not performed.
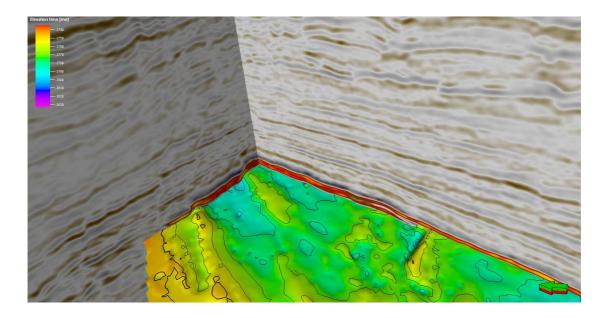

Figure 4-9 the base of the reservoir snapped at the Zero crossing. The top of the red zone represent the top of the reservoir.
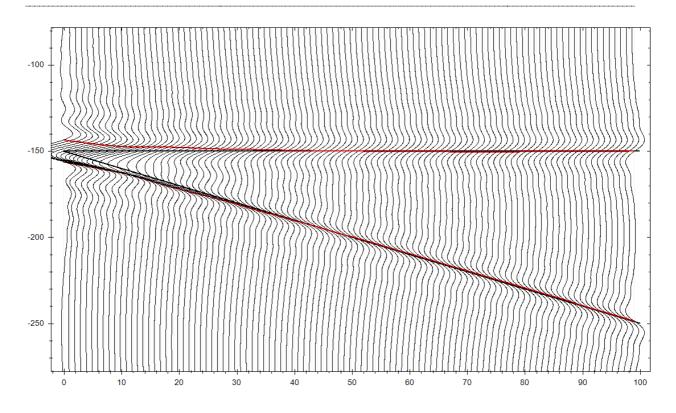
Figure 4-10 A simple band limited impedance wedge used in the detuning process
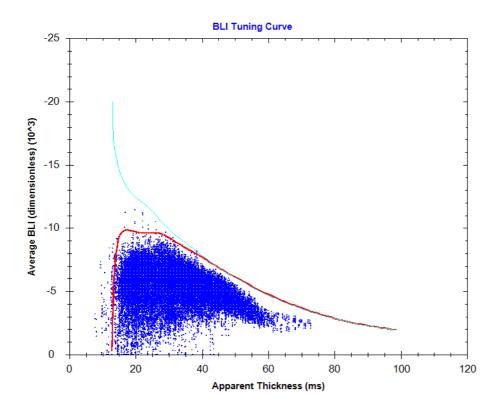

Figure 4-11 Band limited impedance (BLI) tuning curve for 100% net reservoir (red) enveloping the cross plot points of average band limited impedance and apparent thickness. The light blue curve is the calibration amplitude.
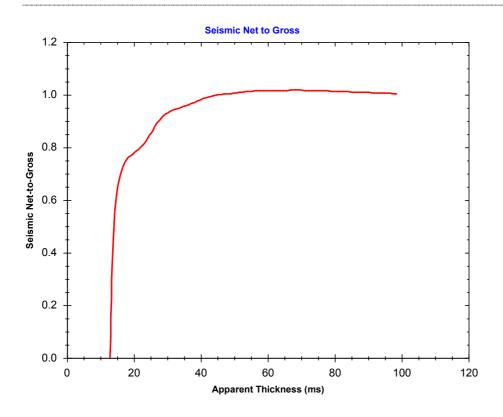
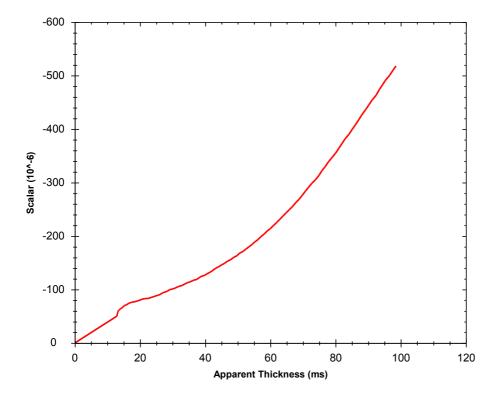Figure 4-12 Seismic net-to-gross curve for the 100 % net reservoir (wedge).

Figure 4-13 The detuning correction curve used in the detuning procedure.

5. RESULTS AND DISCUSSION

In this chapter, the results from the various process and steps will be presented and discussed by using relevant figures.
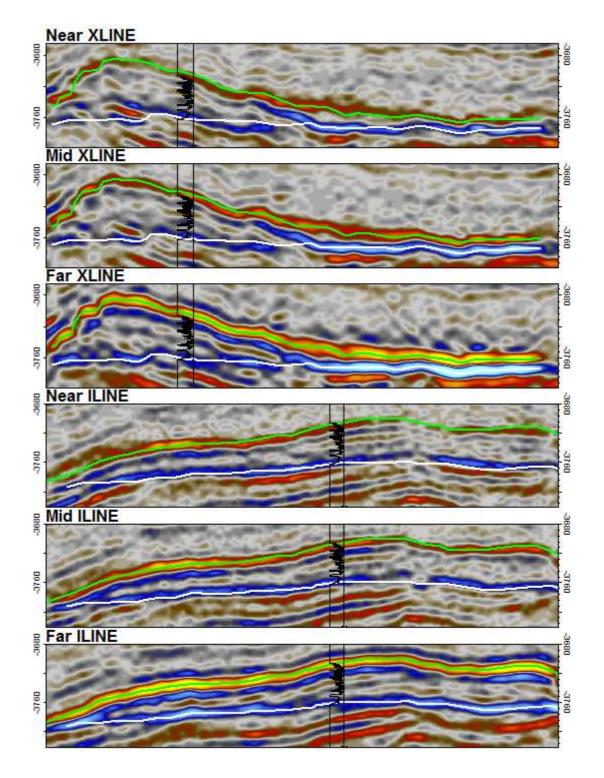
5.1 Results

To make the work complete a brief direct hydrocarbon indicator analysis which enables to decide the presence and extents of hydrocarbon has been conducted and the results are presented below. This will be followed by the presentation of the results of the work flow and the presentation is structured based on the order of implementation in the work flow. Especial emphasis is given to the buildup and generation of the band limited impedance volume which is the base for the final step of the work flow i.e. net pay estimation.

5.1.1   *Hydrocarbon indicator analysis*

Direct hydrocarbon indicators such as bright spots are important features that can provide a quick insight on the presence of hydrocarbon in an area. Bright spots are indicators of remarkable amplitude anomaly, where in relatively soft sand the presence of gas/light oil increases the compressibility of the rock dramatically leading to dropping of velocity and subsequently to decrease in amplitude to a negative bright spot (Avseth, et al., 2005). However, there are other non-hydrocarbon related geological features that can create false bright spot. Examples include volcanic intrusion and volcanic ash layers, highly cemented sandstone, over pressured sands and shale. Since the western margin of the Norwegian Sea is characterized by some volcanic activities, several volcanic seals can be misleading as a bright spot. Discriminating hydrocarbon related bright spots from the false ones require knowledge of the polarity of the seismic data and polarity and AVO responses of the different futures in association to other accompanying futures such as flat spot which should also be verified carefully. The bright spots in the seismic data set have been analyzed to confirm the presence of hydrocarbon.

Figure 5-1 show near, mid and far angle stacks across the well site. The green horizon represents the top of bright spot and we can observe that the amplitude increases with offset. The white pick represent a flat spot, which marks the gas-water-contact. The gas-water-contact is clearly observed in the far offset stack. The polarity reversal at the vicinity of the reservoir in addition to the increase in amplitude with angle and the presence of flat spot

confirm the presence of hydrocarbon and define the limits of the reservoir. This can also be verified with the water saturation log from the petrophysical analysis.

Figure 5-1 Near, mid and far offset stacks showing the bright spot (green) and flat spot (white). Water saturation log is spliced on the seismic. All seismic lines are in the same colour scale, hence brightness represents with amplitude. Negative amplitudes in red and positive one is blues

5.1.2   Extended elastic impedance

The extended elastic impedance enables us to produce the scaled reflectivity as a weighed sum of the intercept and gradient parameterized by the rotation angle χ. To show how the reflectivity changes with χ angle, a series of volumes have been produced.
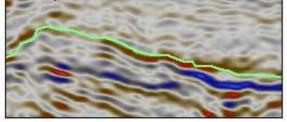
Figure 5-2 shows reflectivity volumes for χ angles 0^0 (intercept), 15^0, 30^0, 45^0, 60^0, 75^0 and 90^0 (gradient). These are reflectivity equivalents to the EEI logs derived from equations at their respective χ angles. The reflectivity varies with the χ angle and the optimal angles representing the elastic and petrophysical properties have been determined based on the strength correlation coefficient. The optimum χ angles determined for fluid and lithology projections are 20 and -50 respectively and are different from those in obtained from the logs.

The scaled reflectivity volumes shale volume and water saturation are produced as weighted sum of the intercept and gradient volumes from the optimal angles (equation [2.9]). Cross lines of far offset stack and the scaled reflectivities for fluid and lithology projection are displayed in Figure 5-3 and Figure 5-4. A clear observation in the figure is that the top of zone of interest is picked uniformly in all the three seismic reflectivities while the base boundary is different on the fluid and lithology reflectivities.
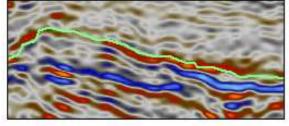
Figure 5-3 display the reflectivities in a cross line along the well location, where the sand in the upper part is filled with gas while sand in the lower part is not gas filled. This part enables us to illustrate the fluid and lithology contacts as the two contacts are different. The sand shale contact is below the gas-water contact hence a fluid cube will image the fluid contact while lithology cube will image the lithological contacts. Figure 5-4 on the other hand display a cross line in the northern part of the reservoir where the all the sand column in the reservoir is filled with gas. In this part it is difficult to differentiate the fluid and lithology contacts based on the fluid and lithology cubes.

The top of the reservoir is reasonable imaged in all the stacks. The base of the gas filled reservoir is clearly imaged in the fluid cube, while the lithology cube images the sand-shale contact. The fluid and lithology cubes along the well location in the inline and crossline directions are displayed in detail in Figure 5-5. The water-gas-contact in the southern boundary of the reservoir (marked in the figure) is reasonably flat and is well defined in the fluid cube while no trace of it is displayed in the lithology cube. Parts of the sand which are not filled with the gas are imaged nicely in the lithology cube.
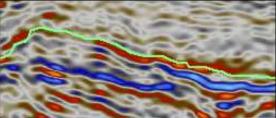
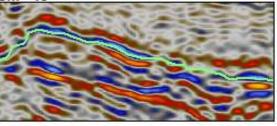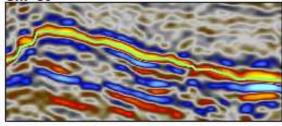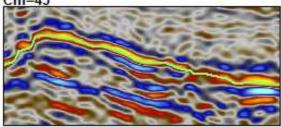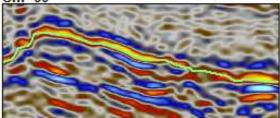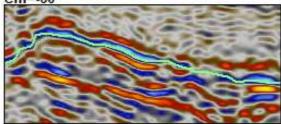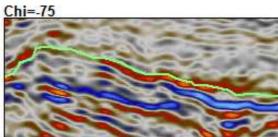Figure 5-2 EEI scaled reflectivity at different χ angles (-90^0 to 90^0)..
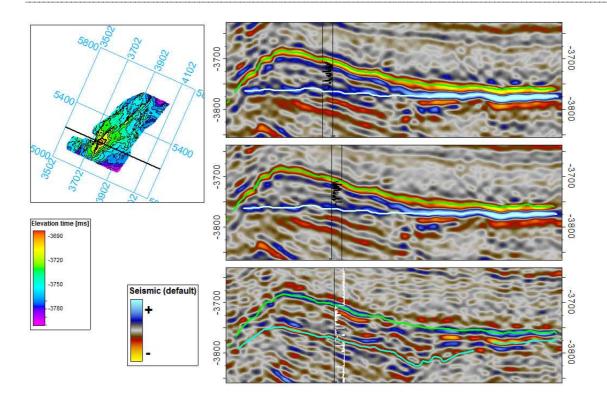
Figure 5-3 Water saturation (white) and shale Vshale (blue) logs spliced on Xline 5216 for A) Far offset (top), fluid (middle) and lithology(bottom) cubes. The top of the reservoir zone is traced by green horizon and the bottom of the reservoir zone by green. The map on the right is the top horizon with the reference for the cross line.
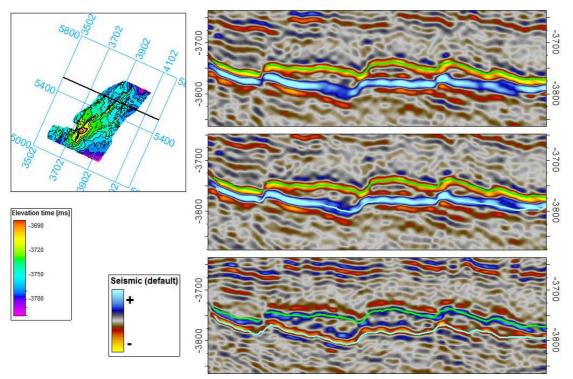

Figure 5-4 A) far offset, B) fluid (B) and C) lithology reflectivities in the gas down to part along cross line 5496
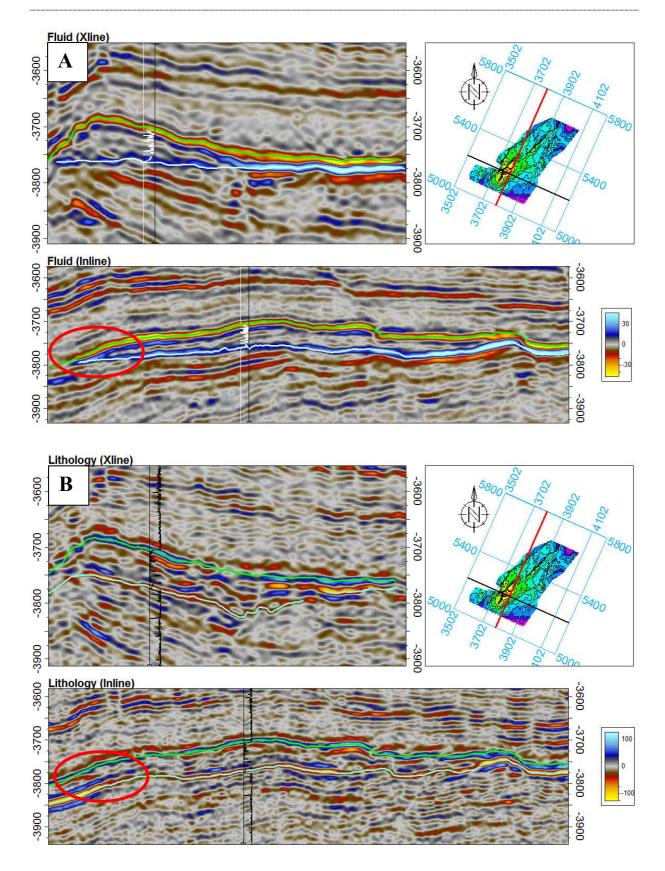
Figure 5-5 Fluid (A) and lithology (B) in crossline 5216 and inline 3790. Water saturation and Vshale logs spliced on the lines. Red circle on the inline shows the flat spot in A and corresponding location in lithology cube.
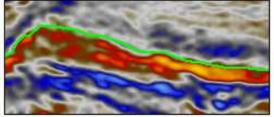
5.1.3   Coloured inversion

Coloured inversion is a deterministic, band limited inversion algorithm which gives relative impedance values. The seismic reflectivity volumes created based on the optimal chi angle were then convolved with the coloured inversion operator (Figure 4-8), which shapes the amplitude spectra of the seismic to the earth's amplitude spectrum, resulting in relative amplitude impedances. The coloured inverted impedances for the series of the EEI reflectivities displayed in Figure 5-2 are presented in Figure 2-1 The peaks and troughs in the seismic reflectivity volumes were transformed to zero crossings and the zone of low impedance represent the reservoir. From the figure, the fluid contacts are imaged in the lower chi angles up to 30^0 and disappear as the angle increases and the lithology contacts start to appear. The internal structure of the reservoir zone varies at different angles.
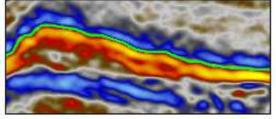
Figure 5-7, Figure 5-8 and Figure 5-9 display the outputs of colour inversion for the far offset stack, fluid and lithology cubes displayed and described in the previous sub section. The band limited impedance for the far offset stack highlighted the gas-water-contacts. Similarly the fluid contact is displayed in the fluid cube; where the base of the gas filled reservoir is clearly defined and the lithology contacts are switch off and no significant low amplitude is displayed below the gas-water-contact. The gas saturated reservoir zone has consistently lower impedance values except some patches of relatively high impedance values in the thicker parts of the reservoir. The fluid cube is used in the reservoir net pay estimation.

The band limited lithology impedance images the lithological contacts. Reservoir sands are imaged clearly and the zone have high band limited impedance values. A direct comparison of the fluid and lithology cubes across and along the well location is displayed in figure 5-9. The fluid cube's impedance values show the boundary of the gas saturated sand in the south (marked in inline). In the northern part where the sands are fully filled with gas the thickness and boundaries of the fluid and lithology are the same, except that the polarity is reversed.
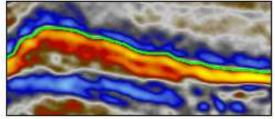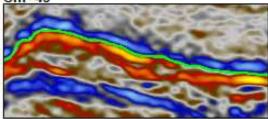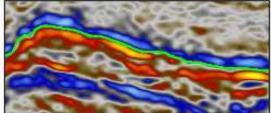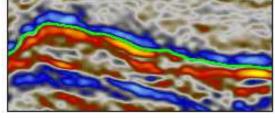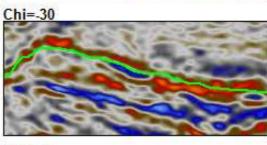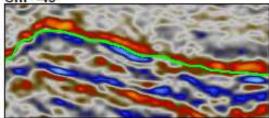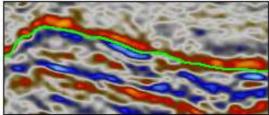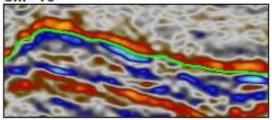
Figure 5-6 Coloured inverted EEI reflectivities at different χ angles (-90^0 to 90^0).
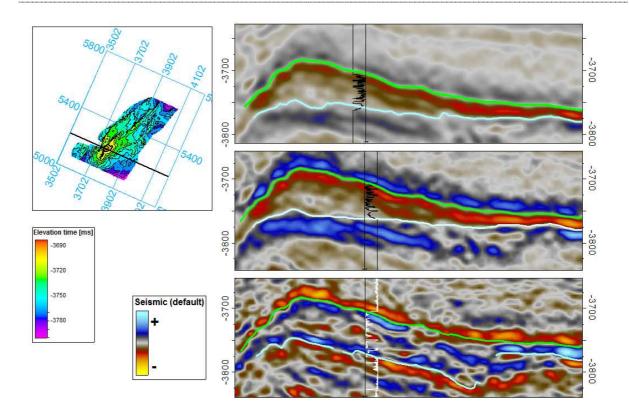
Figure 5-7 The coloured inverted impedance of far offset (top), fluid (middle) and lithology (bottom) cubes across a cross line with Sw (black) and Vshale (white) well logs.
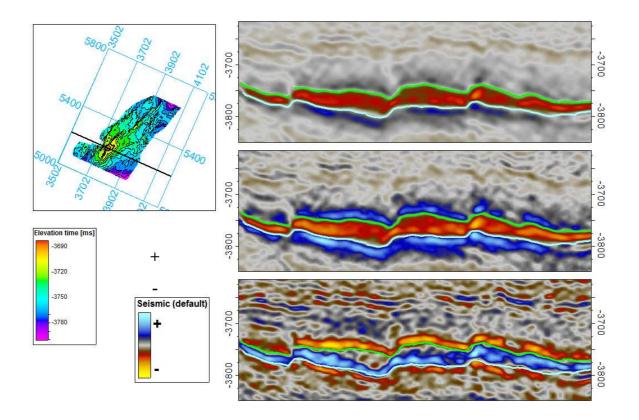
Figure 5-8 The coloured inverted impedance of the fast offset, fluid (middle) and lithology cubes (bottom) across a cross line 5494.
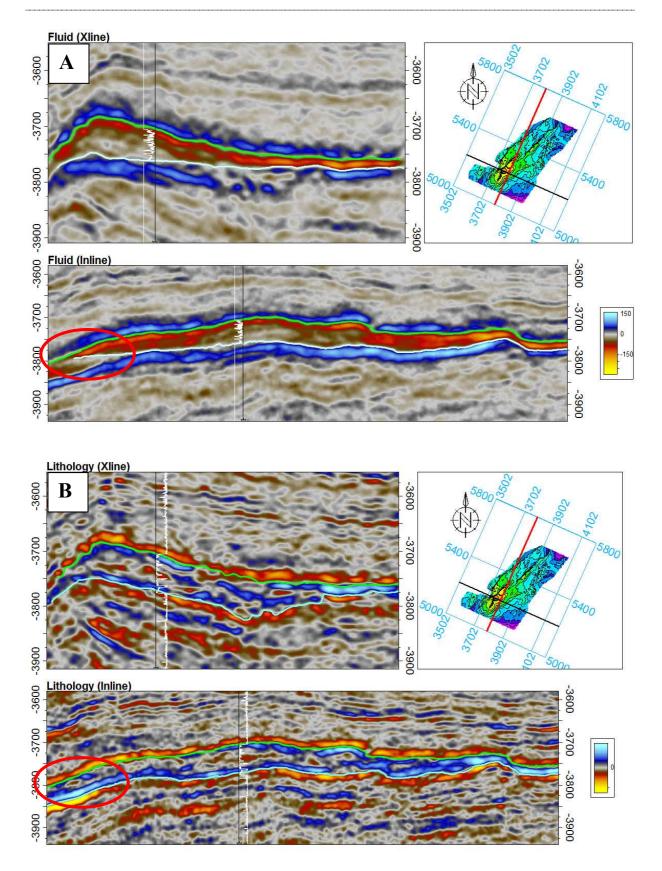
Figure 5-9 Band limited fluid (A) and lithology (B) impedances in cross line (top) and inline (bottom). Water saturation and Vshale logs spliced in fluid and lithology impedances. Redline in the map represents inline and black line represents the cross line.

5.1.4   Net pay estimation

The net pay estimation is based on the average band limited impedance between the zero crossings at the top and bottom of the gas saturated reservoir. The top and base (Figure 5-10) of the zone of interest were snapped to zero crossings. The apparent thickness (Figure 5-10) and the average band limited amplitude were derived between the zero crossings. The maximum apparent thickness is observed at the anticline and decreases out wards. The distribution of the average band limited impedance over the reservoir is displayed in Figure 5-11. The low average impedances (higher negative impedance values) are located in the thinner parts of the reservoir where there is uniformly low impedance. In the thicker part, however the impedance values are higher than those in the thinner. To eliminate the effect of the thickness on the band limited impedance, detuning was applied. As described earlier in the methodology, this is achieved by multiplying the average band limited amplitude by the detuning correction (Figure 4-13) at each apparent thickness. The detuned impedance map is displayed in Figure 5-11 shows that the thicker parts have relatively lower impedance compared to the average band limited impedance and the distribution is quite even.

Once the detuning is performed seismic calibration to associate the band limited impedance with the net pay was performed. The seismic net to gross and the net pay maps are displayed in Figure 5-12. Areas with higher detuned impedance have resulted in high seismic net-to-gross. The net pay which is the product of the net-to-gross and the apparent thickness show thicker net pay areas situated in the central part. Thinner areas in the peripheries of the map, which also have low net-to-pay values, have low net pay thickness. The net pay calucalted in time can be converted to depth given the time-depth relationship and be used in volume estimation calculation.
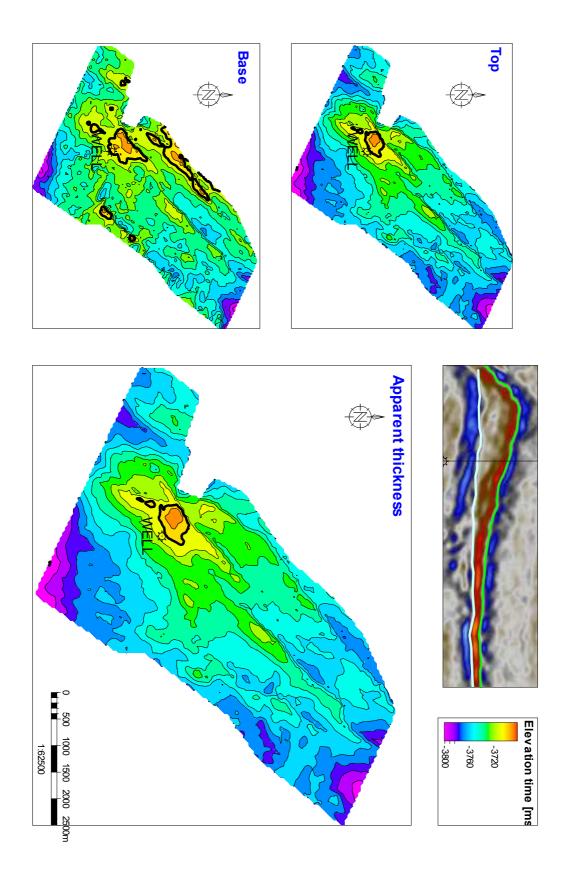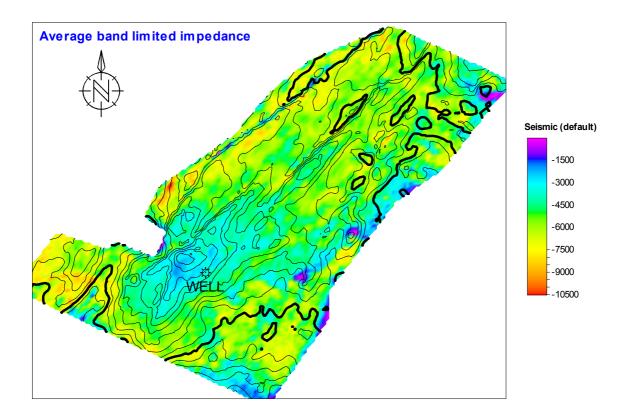
Figure 5-10 The top and base of the reservoir and the apparent thickness between the two. The seismic image at the top shows the top and base picks
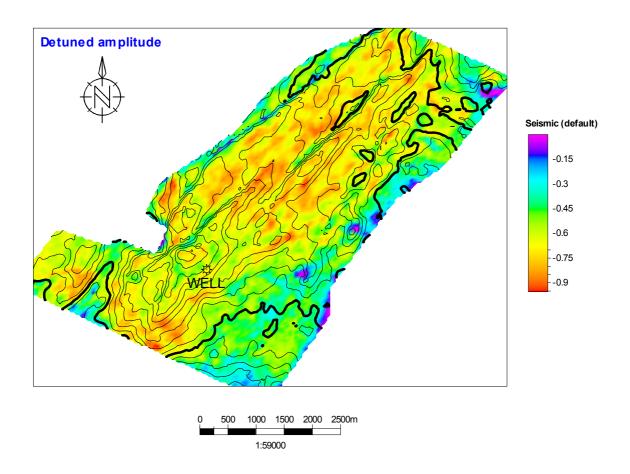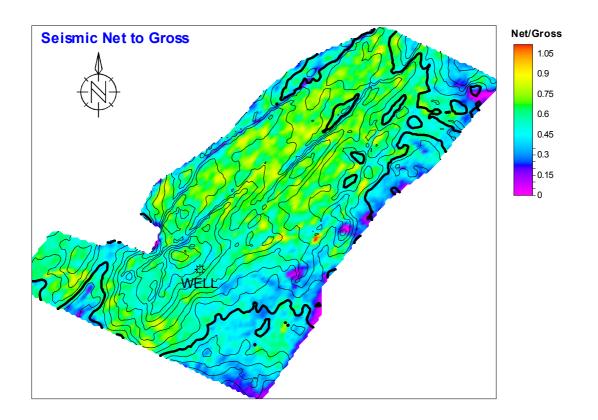
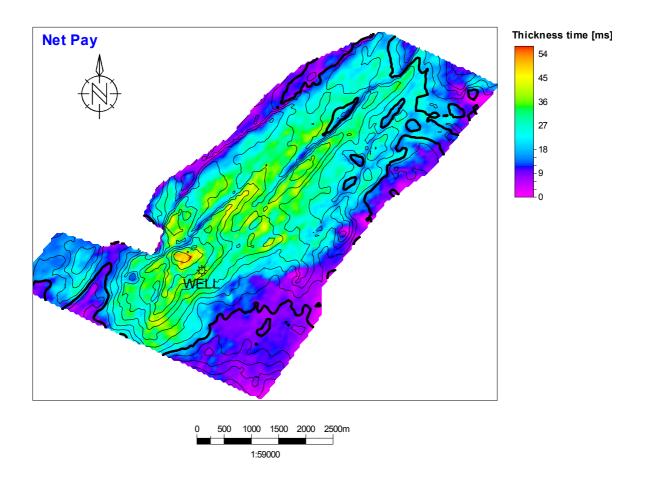Figure 5-11 The average band limited and the detuned impedance.

Figure 5-12 Seismic net-to-gross map (top) is the base to the determination of the net pay (bottom).

5.2 Discussion

The extended elastic impedance is found to be useful in reservoir characterization. The optimal χ angles decided based on the correlation coefficient between the EEI logs and the log of water saturation and the χ angle for the seismic scaled reflectivity are different. It may be related to the quality of the wire line logs and the log-interval over which the EEI is analyzed, noise in the seismic and scaling error in the near-far offsets. Interval of interest has been limited to the reservoir zone and leading to higher correlation coefficient. The seismic may have wrong near-far scaling and this can result in a different optimal angle from the χ angle determined from the well logs. The reflectivities produced from optimal χ angles can still provide good insight of the properties of interest and tuning is required to get a realistic optimal angle.

The top of the zone of interest is reasonably defined in the reflectivity and as well as impedances for both water saturation as well as the Vshale. This is attributed to the fact there is clear impedance contrast at the top, which result in strong reflectivity in the scaled reflectivity and well defined zero crossing. Defining the base is dependent on the property of interest. The fluid differentiate gas saturated zone from brine saturated and the gas-water-contact (Figure 5-1, Figure 5-3 and Figure 5-7) is imaged properly. The gas-water-contact is noticeable on the far offset stack showing that far offset is a reasonable fluid stack for a quick insight. The scaled reflectivity equivalent for the far offset stack (reflection angle, $\theta \approx 30^0$) can be produced at about $\chi=15^0$. This is related to the fact that the bulk modulus is sensitive to fluids. The fluid projection angle in AIGI cross plot is roughly equal to the bulk modulus rotation angle which is usually around 20^0. At this projection angle brine sand impedance will be equal to the shale impedance.

In lithology cube is produced at χ=-50. This is close to the rotation angle of the shear impedance in AIGI domain. The shear impedance is not sensitive to fluid, but is sensitive to the lithology. Since sand have strong shear impedance as compared to shale the blue colour in the lithology cubes can be considered as high shear impedance. Since shear impedance is not sensitive to fluid the gas-fluid contact imaged in the far offset and fluid cube is not visible.

The coloured inversion operator designed contains earth's real spectrum, which is recorded in well log, hence it adjusts the seismic amplitude spectrum to the earth's expected spectrum. This is achieved only within the band limits of the seismic, as the seismic lacks the low and

high frequencies. The band pass frequency filter was applied between 8 and 75 hz. This represents the dominant frequency band width present in the seismic data. The resulting operator show significant amplitude increase in the lower and higher parts of the spectrum, while changes in the middle are relatively lower compared to the original amplitude spectrum of the seismic data (Figure 4-8). A -90 phase rotation was applied to transform the peak and troughs at the reflectors to zero crossings. No additional low frequency was added and the resulting impedances are relative band limited acoustic impedance. Due to the lack of low frequency the impedance values in the thicker part of the reservoir are not fully kept and mix of higher impedance with in low impedance for the fluid and the vice versa for the lithology is the main observation.

The fluid cube (Figure 5-9, A) was used as the base for the net-pay with assumption that the average band limited impedance in the zone of interest is proportional to the net pay if the tuning can be removed. This reflectivity clearly defines one phase (gas) reservoir zone, which is one of the requirements for the efficient implementation of the net pay algorithm.

The net pay estimation is based on the attributes apparent thickness and average band limited impedance. Detuning and calibration are integral part of the algorithm. A band limited impedance wedge model is used in the detuning the tuning effect on the band limited impedance. The detuning in the net-pay estimation boosted the contribution of the average band limited impedance in the thicker parts. The detuning correction increases with thickness (Figure 4-13) and it is also evident on the map (Figure 5-11). The slop of the detuning correction depends on the lower frequency component, which means there is a limit on the maximum apparent thickness that can be used in the estimation. This thickness is equivalent to the half cycle of the frequency. The lowest frequency both in the coloured inversion impedance and the filter used to build the band limited impedance wedge is 8 Hz. Hence, estimates in the thickest parts could be beyond the efficiency level of the algorithm. However, given the well data on the lithology, the thicker areas in the anticline are expected to have higher net pay thickness. Seismic calibration was manually performed by fitting the tuning curve for the 100% reservoir case, to envelop the data appoints in the apparent thickness versus average band limited amplitude crossplot.

Assessments of uncertainty in the estimation was not performed in this work, but conducting the uncertainty procedures dealt in Connolly and Kampers (2007) would allow the quantification of the various uncertainties associated with seismic reservoir characterization.

CONCLUSION

The work flow is found to be useful for fast track seismic reservoir characterizing. The extended elastic impedance is a good way to link the log petrophysical properties with seismic data. The possibility to emphasize the properties of interest such as fluid and lithology projection makes it a power full tool in seismic reservoir characterization. The optimal angle in log and seismic data can be different and hence additional tuning is required to gain the optimal χ angle in seismic data. The fluid and lithology cubes were produced $\chi = 20^0$ and $\chi = -50^0$ respectively.

The coloured inversion is found out to be simple, and fast technique requiring the power low exponent, α and knowledge of the frequency band limit. A single coloured inversion operator was designed and the scaled reflectivities. The amplitude reshaping is based on the well log; hence it represents valuable information about the earth's spectrum. No low frequency was added in the inversion algorithms and the output lacks the low frequency component. This is particularly evident in the thicker parts of the reservoir.

Net-pat estimation was made based on the fluid cube. The net-pay estimation based on band limited impedance of the fluid cube was out to be simple but effective method. The selection of wavelet to build the wedge model is important factor in the efficiency of the method. The ability to handle complex wavelet is doubtable as the resulting tuning curve and detuning correction functions were quite complicated. The knowledge about lower frequency component, the accuracy of zero crossing picks, the presence of one or more phase are all important and proper consideration is required for the successful application of the seismic net pay algorithm.

The work flow can be applied in a simple step by step approach and when used with the assessment of uncertainty, it can provide a tool in exploration reducing risk as associated with exploration appraisal wells.

REFERENCES

Aki, K. I. & Richards, P. G., 1980. *Quantitative Seismology.* San Francisco: W. H. Freman & Co..

Arsalan, S. I. & Yadav, A., 2009. Application of extended elastic impedance: A case study from Krishna-Godavari basin, India. *Leading Edge,* pp. 1204-1209.

Avseth, P., Mukarji, T. & Mavko, G., 2005. *Quantitative Seismic Interpretation.* Cambridge: Cambridge University Press.

Bacon, M. & R. Simm, T. R., 2003. *3D Seismic Interpretation.* 1st ed. Cambridge: Cambridge Univerity Press.

Bortfeld, R., 1961. Approximation to the reflection and transmission coefficients of plane longitudinal and transverse wave. *Geophysical Prospecting ,* Volume 9, pp. 485-502.

Brekke, H., Dahlgren, S., Nyland, B. & Magnus, C., 1999. The prospectivity of the Vøring and Møre basins on the Norwegian Sea continental margin. In: A. Fleet & B. S. A. R., eds. *Petroleum Geology of Northwest Europe, Proceedings of the 5th Conference.* London: Geological Society, pp. 261-274.

Brown, A. R., Wright, R. M., Burkart, D. & Abriel, W. L., 1984. Interactive seismic mapping of net producible gas sand in the Gulf of Mexico. *Geophysics,* Volume 49, pp. 686-714.

Connolly, P., 1999. Elastic Impedance. *The Leading Edge,* 18(4), pp. 438-542.

Connolly, P., 2007. A simple, robust algorithm for seismic net pay estimation. *Leading Edge,* pp. 1278-1282.

Connolly, P. & Kemper, M., 2007. Statistical uncertainty of seismic net pay estimations. *Leading Edge ,* Volume 26, pp. 1284-1289.

Connoly, P., 2010. *Robust Workflows for Seismic Reservoir Characterisation,* s.l.: SEG Distinguised Lectures Series.

Fonneland, H. C. et al., 2004. Deterital zircon ages: a key to undertanding the deposition of deep marine sandstones in the Norwegian Sea. *Sedimentary Geology,* Volume 164, pp. 147-159.

Lancaster, S. & Whitcombe, D., 2000. Fast-track 'coloured' inversion. *SEG Expanded Abstract.*

Latimer, B., Davdson, R. & R. Van, R., 2000. An interviewer's guide to undestanding and working with seismic-derived acoustic impedance data. *The Leading Edge,* Issue 3, pp. 242-256.

Lien, T., 2005. From rifting to drifting: effects on the development of deep-water hydrocarbon reservoirs in a passive margin setting, Norwegian Sea. *Norwegian Journal of Geology,* Volume 85, pp. 319-332.

Neff, D. B., 1993. Amplitude map analysis using forward modelling in sandstone and carbonate reservoirs. *Geophysiscs,* Volume 58, pp. 1428-1441.

Pennington, W., 2001. Reservoir Geophysics. *Geophysics,* Issue 1, pp. 25-30.

Ritter, U. et al., 2004. Heat flow in the Vøring Basin, Mid-Norwegian Shelf. *Petroleum Geoscience,* Volume 10, pp. 353-365.

Schramm, J. M. W., Dedman, E. V. & Lindsey, J. P., 1977. Practical stratigraphic modeling and interpretation. In: C. E. Payton, ed. *Seismic Stratigrahy- Applications to Hydrocarbon Exploration (AAPG Memior 26).* s.l.:AAPG, pp. 477-502.

Shuey, R., 1985. A simplification of Zoeppritz equations. *Geophysics,* Volume 50, pp. 609-614.

Simm, R., 2009. Simple net pay estimation from seismic: a modelling study. *First Break,* pp. 45-53.

Simm, R., White, R. & Uden, R., 2000. The anatomy of AVO crossplots. *The Leading Edge,* 19(2), pp. 150-155.

Smith, G. C. & Gidlow, P., 1987. Weighted satacking for rock propertly estimation and detection of gas. *Geophysical Prospecting,* pp. 915-942.

Talling, P. J., 2001. On the frequency distribution of turbidite thickness. *International Association of Sedimentologists,* Issue 48, pp. 1297-1329.

Whitcombe, D. N., 2002. Normalizing Elastic Impedance. *Geophysics,* 67(1), pp. 60-62.

Whitcombe, D. N., Connolly, P. A., Reagen, R. L. & Redshaw, T. L., 2002. Extended elastic impedance for fluid and lithology prediction. *Geophysics,* Volume 67, pp. 63-67.

Zeng, H. L. & Backus, M. M., 2005. Optimize thin-bed interpretation with 90° - phase wavelets. *SEG Expanded Abstracts,* pp. 790 - 793.